Facile and scalable fabrication of high-energy-density sulfur cathodes for pragmatic lithium-sulfur batteries

Min-Seop Kim[a,b], Mun Sek Kim[a], Vandung Do[a,c], Yongyao Xia[d], Woong Kim[b,*], Won Il Cho[a,c,**]

[a] Center for Energy Storage Research, Korea Institute of Science and Technology, Seoul, 02792, Republic of Korea
[b] Department of Materials Science and Engineering, Korea University, Seoul, 02841, Republic of Korea
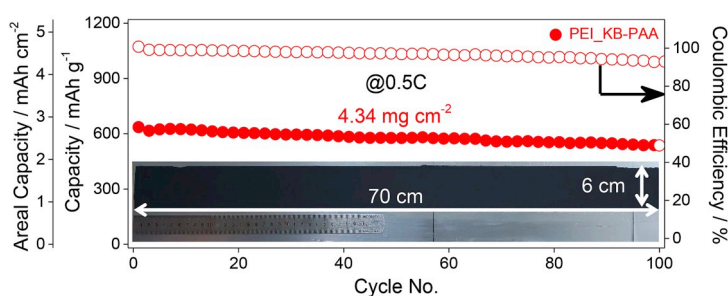[c] Division of Energy and Environmental Technology, Korea University of Science and Technology, Daejeon, 34113, Republic of Korea
[d] Department of Chemistry and Shanghai Key Laboratory of Molecular Catalysis and Innovative Materials, Institute of New Energy, IChEM (Collaborative Innovation Center of Chemistry for Energy Materials), Fudan University, Shanghai, 200433, China

HIGHLIGHTS

- Scalable synthesis of PEI-functionalized KB (PEI_KB) as a sulfur host is feasible.
- Combining the PEI_KB and PAA enables to produce the stable high-S-loading cathodes.
- Large-dimension ($70 \times 6 \, cm^2$) cathode with S loading of $> 4.3 \, mg \, cm^{-2}$ is prepared.
- Cathode with 12 wt% of PEI in PEI_KB shows durable cycling over 600 cycles at 1C.
- The 12PEI_KB-PAA cathode presents a high areal capacity of $4.64 \, mAh \, cm^{-2}$ at 0.1C.

GRAPHICAL ABSTRACT

ARTICLE INFO

ABSTRACT

Lithium-sulfur battery is garnering much of attention due to its high energy densities, low-cost active material of sulfur and variety of applications in portable electronics. High integrity and consistent qualities of the large-scale sulfur cathode with high energy have to be ensured to construct reliable and practical lithium-sulfur batteries that could supersede advancing lithium-ion batteries. Here, facile and productive approaches are developed to mass-produce functional sulfur hosts and to fabricate large-scale sulfur cathode with high sulfur loading. The functional sulfur host is synthesized by anchoring polyethylenimine at the surface of commercially available carbon at inert conditions with a scale of more than 10 g per batch via simple solution method. Combining the functionalized sulfur host with a polyacrylic acid binder allows high integrity and uniformity of the high sulfur loading cathode to be fabricated in large dimensions. Followed by this approach, the sulfur cathode, $70 \times 6 \, cm^2$, is produced with the sulfur loading of $> 4.3 \, mg \, cm^{-2}$. It is found that 12 wt% of polyethylenimine in the functionalized sulfur host with polyacrylic acid is at optimal condition that presents stable electrochemical performances over 600 cycles.

---

* Corresponding author.
** Corresponding author.
E-mail addresses: woongkim@korea.ac.kr (W. Kim), wonic@kist.re.kr (W.I. Cho).

1. Introduction

Lithium-sulfur (Li−S) batteries are considered as a promising candidate to supplant conventional lithium-ion batteries (LIBs) in energy storage industries especially for applications in electric vehicles (EVs). This is because Li−S batteries have a high theoretical specific capacity of 1675 mAh g^{-1} and an energy density of ~2600 Wh kg^{-1}; these values are approximately seven times larger than those of conventional LIBs [1,2]. Furthermore, elemental sulfur (S_8) is attractive for an active material because of its low cost and abundance. Nevertheless, several inherent complications of Li−S chemistries such as poor cyclability and passivation of the anode and cathode are induced by the dissolution and random migration of intermediate reactant species of lithium polysulfides (LiPSs) during the redox processes, so-called LiPS shuttling [3–6]. Extensive studies have been reported based on various strategies to resolve the intrinsic problems associated with Li−S batteries [4,5,7–11]. However, Li−S batteries are still far from to be mass-produced for the applications in EVs industries because most of these works have been carried out in a lab-scale with the utilization of low-energy-density sulfur cathodes, with densities of less than 2 mg cm^{-2}. Besides, further safety issues that are being thoroughly investigated in LIBs due to worldwide concern have not yet been adequately considered in Li−S batteries [12,13]. To achieve an energy density corresponding to the areal capacity of 4 mAh cm^{-2} in current LIBs, which is the minimum requirement for the EVs industries, it is necessary to develop mass producible high-energy-density sulfur cathodes with enhanced sulfur loading amount greater than 5 mg cm^{-2} to fabricate the reliable Li−S batteries [14–16].

Many sulfur host materials have been rationally developed to improve utilization rate and reversibility of elemental sulfur in Li−S batteries. The most widely adopted sulfur host materials are 1-dimensional (1D) carbon nanomaterials, including carbon nanotubes (CNTs) and nanofibers (CNFs). Various configurations for forming sulfur composites with CNF cloth [17], hierarchical CNT paper [18] and porous CNF layers [19] have been developed for ultrahigh-sulfur-loading cathodes. In addition, 2D graphene materials [20–22] and porous carbon sphere materials [23] are utilized in combination with 1D carbon materials. Despite the promising features of the developed sulfur hosts, it is understood that the materials are impractical to be employed for constructing actual Li−S batteries at the current stage. These limitations mainly arise from cumbersome synthesis process of the materials, infeasibility of mass production of the active materials and inconsistent quality control of the high energy sulfur cathode fabrications at large dimensions. Also, limited C-rate performances of Li−S batteries, due to low utilization rate of insulating sulfur, hinder the further practical development of these rationally designed materials. In addition, most of the studies have reported unique sulfur host materials in the form of free-standing cathodes without a conventional Al foil current collector. Free-standing sulfur cathodes mainly made of carbonaceous materials are not suitable for metal-tab welding in subsequent production at the pouch-cell level for actual fabrications of Li−S batteries [16,24].

Focusing on the fabrication of practical and productive high-sulfur-loading cathodes with commercial sulfur host materials and with Al current collector is essential for the further progress of Li−S batteries to be employed in EVs and many other applications. Among available sulfur hosts, Ketjen black (KB) is promising as a practical sulfur host due to its commercial applicability with unique carbon properties: the unique properties of KB, a nm-scale particle size and high specific surface area (SSA), ~1400 m^2 g^{-1}, could provide a sufficient high active SSA with high conductivity to allow more sulfur to be utilized and deliver a high discharge capacity [25,26]. Furthermore, KB is advantageous in facilitating the production of large-scale sulfur cathodes due to its convenience for use at a bulk scale, as this material is already mass produced at a low price (20–60 $ kg^{-1}). Since it is imperative to evaluate electrochemical properties of sulfur cathodes at the pouch-cell

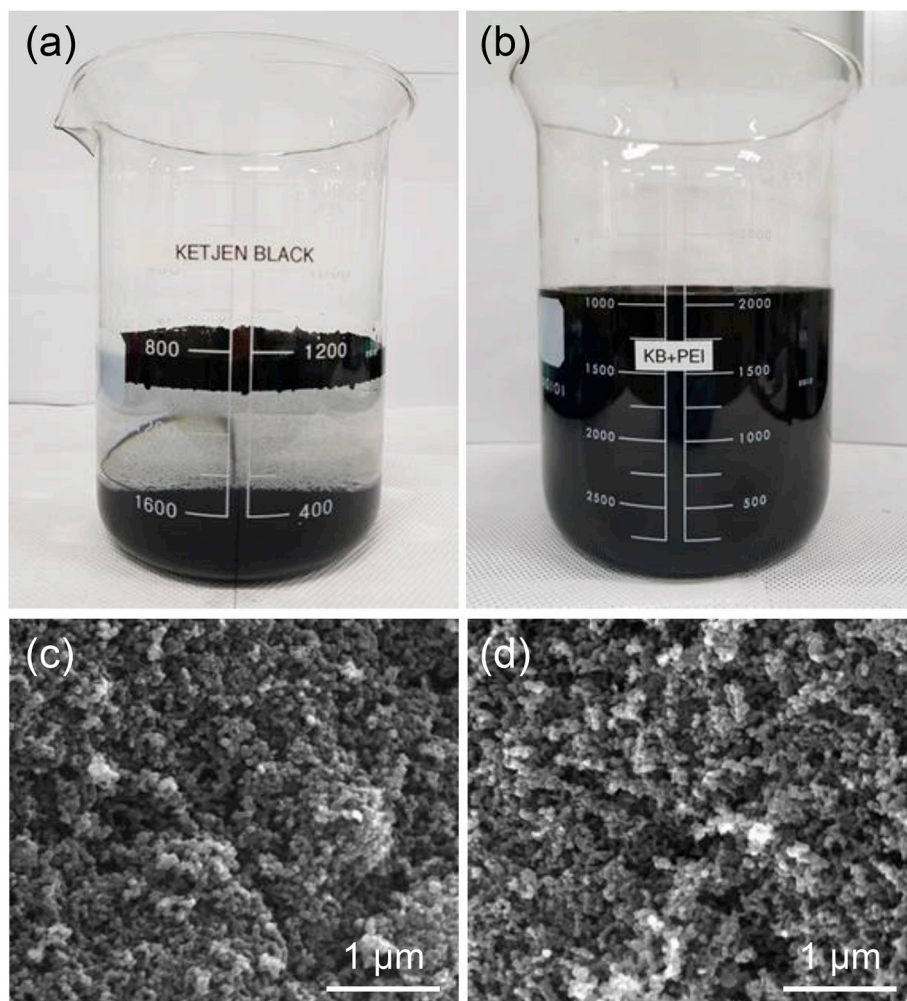level, large-scale sulfur cathodes that are consistent in qualities must be easy to be manufactured.

Few studies have been performed on the use of KB for the sulfur host to make large-scale sulfur cathodes with high sulfur loadings due to the low mechanical integrity. The high SSA and nonpolar surface nature of KB provoke severe aggregation and volume shrinkage during the cathode fabrication process, followed by a large amount of surface fissure and delamination [15,27]. The typical approach is the synthesis of microsized and cross-linked secondary structures consisting of the primary KB particles. Xiao et al. designed a cross-linked integrated KB (IKB) by the carbonization of KB and citric acid and produced a cathode with a sulfur loading of 3.5 mg cm^{-2} and no cracking or delamination [15]. Zhang et al. showed a similar strategy with KB and gelatin to synthesize a cauliflower-like electrode material for solid cathodes with a high sulfur loading of up to 14 mg cm^{-2} [27]. However, both studies produced successful electrochemical performance only at very low current densities, such as 0.1C and 0.01C, respectively, and Zhang et al.'s work developed primary batteries. Furthermore, Choi and Kim et al. employed KB as a main sulfur host material for a high-sulfur-loading cathode with a sulfur loading of 3 mg cm^{-2} [28]. Although the cathode delivered good electrochemical cycle performance at 0.5C, increased binder amount was used to enhance the adhesion between the slurry and the current collector. Ultimately, the most important consideration in making a high-sulfur-loading cathode using KB as the sulfur host is maintaining the cathode's integrity with current collectors.

In this study, we demonstrate that facile surface functionalization of the KB, commercial grade sulfur host, with polyethylenimine (PEI, PEI_KB) and utilization of polar polyacrylic acid (PAA) binder to enable fabrication of large-scale and high-sulfur-loading cathodes for constructing reliable Li−S batteries. PEI is the amine-rich polymer that can functionalize CNTs, which enables applications in various fields, such as CO_2 reduction [29], synthetic interfering RNAs [30], and supercapacitors [31]. Additionally, multi-amine functional groups of PEI function efficiently in Li−S batteries as positively charged amine species can electrostatically attract negatively charged LiPSs [32]. Furthermore, PEI_KB facilitates the manufacturing of large-scale and high-energy-density sulfur cathodes by not only preventing the aggregation of KB but also interacting robustly with the PAA binder for enhancing an adhesion. Here, a high-sulfur-loading cathode with the sulfur loading of > 4.3 mg cm^{-2} and with the dimension of 70 × 6 cm^2 composed of PEI_KB sulfur host and PAA binder (PEI_KB-PAA) have been employed. On top of that, simple ball milling process is done instead of thermal infusion of elemental sulfur to practically fabricate the sulfur composite with PEI_KB. The optimal ratio of 12 wt% PEI in PEI_KB with PAA binder demonstrates the durable electrochemical cycle performance over 600 cycles. Furthermore, the fabricated high-sulfur-loading cathode exhibits an areal discharge capacity of 4.63 mAh cm^{-2} at 0.1C and a stable cyclability of over 100 cycles at 0.5C with a retention ratio of above 85%.

2. Experimental section

2.1. Materials

KB (EC600JD) was purchased from Lion Specialty Chemicals. Vapor-grown carbon fiber (VGCF) was purchased from Showa Denko. Multiwalled carbon nanotubes (MWCNTs) were provided by Hanwha Chemical. Elemental sulfur (99.98%), PEI polymer (MW ~ 250,000), PAA (MW ~ 250,000), N-methyl-2-pyrrolidone (NMP), lithium nitrate (LiNO$_3$), 1,2-dimethoxyethane (DME), and 1,3-dioxolane (DOL) were purchased from Sigma-Aldrich. Polyvinylidene fluoride (PVdF) was purchased from SOLVAY. Lithium bis(trifluoromethanesulfonyl)imide (LiTFSI) salt was purchased from 3 M.

Fig. 1. Digital photographs of PEI_KB synthesis steps: (a) addition of KB to D.I. water and (b) PEI_KB after reaction. SEM images of (c) KB powder and (d) PEI_KB composite powder.

2.2. Fabrication of PEI_KB composites

Two separate solutions were prepared to synthesize the PEI_KB composite powder. First, KB powder was dispersed in deionized (D.I.) water at a concentration of $10\,mg\,mL^{-1}$ by ultrasonication (500 Watt) for 30 min. Then, the PEI polymer was completely dissolved in D.I. water separately. After completely dissolving the PEI, the prepared KB and PEI solutions were homogeneously mixed by vigorous stirring in an 80 °C oil bath for 24 h. Then, the solution was filtered and washed with D.I. water several times to eliminate the residual PEI polymer thoroughly. Afterward, the PEI_KB composite powder was obtained by drying the filtered powder in an 80 °C oven overnight. In this study, three different PEI solutions were prepared with concentrations of $1\,mg\,mL^{-1}$, $5\,mg\,mL^{-1}$, and $10\,mg\,mL^{-1}$ to adjust the corresponding PEI ratios in PEI_KB composites. These composites are denoted here as 7PEI_KB, 12PEI_KB, and 25PEI_KB, according to the corresponding PEI weight ratios of 7 wt%, 12 wt%, and 25 wt%, respectively.

2.3. Material characterization

The crystal structure of the materials was characterized by X-ray diffraction (XRD, D/MAX 2500/PC, Rigaku). The morphology was observed by scanning electron microscopy (SEM, Inspect F50, FEI). The Brunauer-Emmett-Teller (BET) surface area and total inner pore volume were obtained by N_2 adsorption-desorption isotherms collected at 77 K (BELSORP-max, BEL), and the pore size distribution was calculated

based on a nonlocal density function theory (NLDFT) method. Raman spectra were collected using a 532 nm Nd: Yag laser source (In Via Raman Microscope, Renishaw). X-ray photoelectron spectroscopy (XPS) was carried out using a monochromator with Al Kα (1486.6 eV) X-ray radiation (PHI 5000 VersaProbe, Ulvac-PHI). Thermogravimetric analysis (TGA) was measured under N_2 flow ($100\,mL\,min^{-1}$) from room temperature to 800 °C at a heating rate of $10\,°C\,min^{-1}$ (SDT Q600, TA Instrument).

2.4. Electrochemical measurements

The cathode slurry was prepared by homogeneously mixing elemental sulfur, PEI_KB, VGCF, and PAA at a weight ratio of 60:20:10:10 by ball milling. D.I. water was added to adjust the viscosity of the slurry. Subsequently, the slurry was cast on Al foil (15 μm thick) current collector and dried in a vacuum oven at 80 °C overnight to remove the solvent. The areal sulfur loading amounts of the prepared cathodes (PEI_KB-PAA) were up to $4.34\,mg\,cm^{-2}$. A control sulfur cathode (KB-PAA) using KB powder instead of PEI_KB was fabricated as well, via the same procedure, with a sulfur loading up to $4.3\,mg\,cm^{-2}$. For further comparison, a cathode composed of KB and PVdF binder (KB-PVdF) was also fabricated with a weight ratio of S:KB:PVdF = 60:30:10 with NMP as a solvent. The ether-based liquid electrolyte was prepared by dissolving 1.0 M lithium bis(trifluoromethanesulfonyl)imide (LiTFSI) and 0.2 M lithium nitrate ($LiNO_3$) as an additive in a 1,2-dimethoxyethane (DME) and 1,3-dioxolane (DOL) cosolvent with a volume ratio of 1:1.

The CR2032 coin-type cell was assembled using a 12 mm diameter disk-type sulfur cathode, lithium metal anode, electrolyte, and Celgard 2500 separator. A 40 μL aliquot of liquid electrolyte was injected, and the electrolyte/sulfur ratio was approximately 10 (μL mg^{-1}). The galvanostatic electrochemical properties of the sulfur cathodes were investigated through a battery cycler system (MACCOR Series 4000) in the potential range of 1.5–2.7 V (vs. Li/Li$^+$). Cyclic voltammetry (CV) was performed on VMP3 (BioLogic) within a voltage window of 1.5–2.8 V (vs. Li/Li$^+$) at 0.1 mV s^{-1} scan rate. Electrochemical impedance spectroscopy (EIS) measurements were performed with the same VMP3 in a frequency range of 500 kHz to 100 mHz with an amplitude of 7.1 mV. Each spectrum was measured before cycling (at OCV) and after 1st discharge-charge cycle.

3. Results and discussion

3.1. Large-scale synthesis of the functional sulfur host

The large-scale synthesis of PEI_KB composite, using above 10 g of KB per batch (Fig. S1), is carried by one-step solution method (Fig. 1). Although porous and conductive carbon is essential for applications in various fields, hydrophobic surface characteristics of carbon induce particle aggregation problems. Due to high porosity and nonpolar surface feature of KB, 10 g of KB is poorly dispersed in 1000 mL of D.I. water not only immediately after the addition but also after ultrasonication (Fig. 1a). However, merely mixing the KB-D.I. water mixture with a PEI solution in an 80 °C oil bath produces a well-dispersed solution of PEI-surface-functionalized-KB without any aggregation of KB due to attachment of polar amine groups of PEI at KB (Fig. 1b). The change in dispersity indicates that the surface features of KB have been changed after the functionalization with PEI. Although the surface of KB became more polar, the morphology of the PEI_KB composite remains unchanged compared to the KB (Fig. 1c and d). Furthermore, controlling the weight fraction of PEI in the PEI_KB composite from 7 wt % to 25 wt%, which are confirmed by TGA (Fig. S2), is performed by adjusting the limiting amount of PEI reactant in the functionalization step. As shown in Fig. 1, both the scaled-up production and uniform distribution of PEI_KB are achieved.

3.2. Characterizing surface properties and structures of PEI_KB

XPS analysis is performed to confirm the attachments of PEI on KB (Fig. 2). After the attachment, evident N1s (400 eV) peak is observed for PEI_KB in the XPS survey-scan spectrum, indicating the complete attachment of PEI on the KB (Fig. 2a). The increase in the peak at 285.9 eV is due to the presence of C−O bonds and the C−N bonds on the main chain of PEI (Fig. 2b and c). Deconvolution of the N1s (Fig. 2d) exhibits the presence of N−C═O binding (402.0 eV) and a residual amine group, as indicated by N−C (399.5 eV) and N−H (400.0 eV) bindings [22]. Archer et al. have used carboxylic-acid-functionalized MWCNTs (MWCNTs-COOH) to tether PEIs via interactions between the PEIs and hydroxyl and/or carboxyl functional groups [9]. Compared with the C1s peaks of KB (Fig. 2b) and MWCNTs (Fig. S3), KB has higher relative area intensities of C−O hydroxyl bonding (286.2 eV) and O−C═O carboxyl bonding (288.6 eV) than those of MWCNTs based on the respective C1s spectra (Table S1). Considering the scalability of the sulfur host, however, it is difficult to scale-up the sulfur host with MWCNTs-COOH because of its high price, which is substantially higher than that of KB. Therefore, adopting KB is advantageous for the cost-effective large-scale synthesis of PEI-functionalized carbonaceous material for sulfur hosts.

XRD, Raman, and BET measurements are used to characterize the structure of the prepared PEI_KB (Fig. 3). The XRD results (Fig. 3a) of KB and PEI_KB present two diffraction peaks at 23.4° and 43.2°, which correspond to the (002) and (101) graphitic planes, respectively (JCPDS #75–1621). These two characteristic peaks originate from the graphitic structure of both high-electrical-conductivity carbon materials. Raman spectroscopy also shows a G band (1593 cm^{-1}) caused by the graphitic structure of all carbon samples (Fig. 3b) [33]. Furthermore, 2D (∼2700 cm^{-1}) and D + G band (∼2910 cm^{-1}) are observed due to the presence of a graphitic layer in both KB and PEI_KB [34,35]. Overall, the Raman spectra and I$_D$/I$_G$ integrated area ratio of KB and PEI_KB are comparable, which indicates no influence on the KB structure after the PEI attachment. An apparent difference is found in the results of N$_2$-isotherm measurements (Fig. 3c). In the N$_2$-isotherm results, KB shows a type IV adsorption-desorption curve (according to IUPAC classification) with a hysteresis loop, which is attributed to the mesopore structure of the material [36]. After PEI attachment, however, the adsorption-desorption curve changes to type I, consisting of mainly a micropore structure, as a result of PEI occupying most of the mesopore volume of KB within the agglomerates of primary KB particles [37]. This result is consistent with the pore size distribution (PSD) results (Fig. 3d) based on the NLDFT, which is a more precise calculation of PSD when the calculation focuses on micro- and meso-pores [38]. As
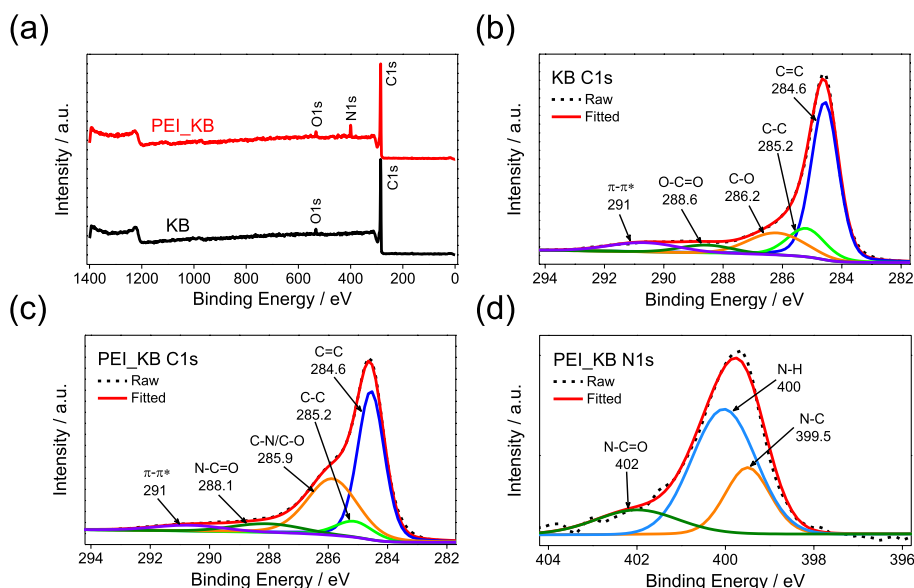

Fig. 2. Results of XPS analyses: (a) survey spectra of PEI_KB and KB; high-resolution XPS spectra of (b) C1s of KB, (c) C1s of PEI_KB, and (d) N1s of PEI_KB.
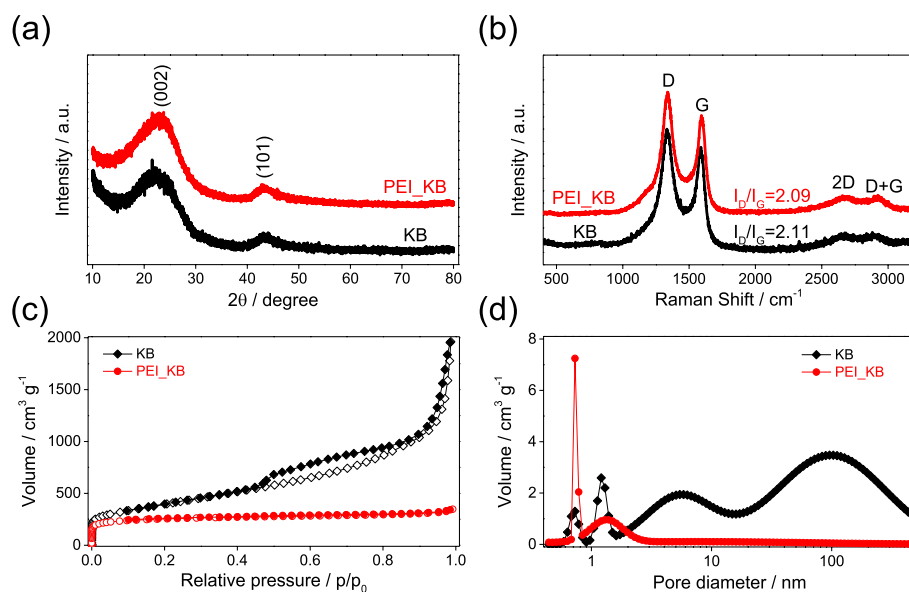
Fig. 3. (a) XRD patterns, (b) Raman spectra, (c) N_2 isotherms, and (d) pore size distributions of PEI_KB and KB.
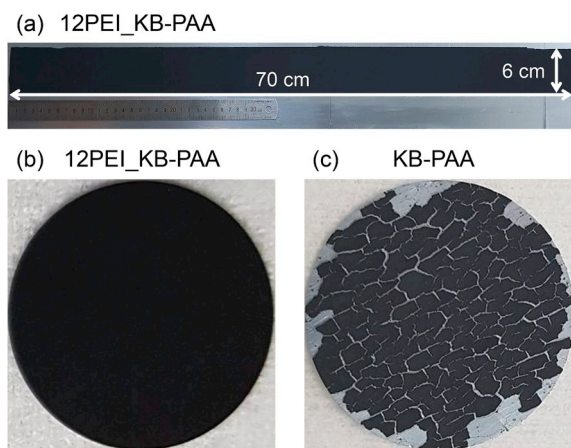

Fig. 4. Top-view digital photographs: (a) fabricated large-area cathode composed of PEI_KB-PAA and the cathodes after punching in a disk shaped (b) PEI_KB-PAA and (c) KB-PAA (S loading of all cathodes > 4.3 mg cm^{-2}).

shown in Fig. 3d, the mesopore and macropore volumes of PEI_KB have disappeared. Therefore, the SSA and total inner pore volume of PEI_KB are decreased to 937.8 m^2 g^{-1} and 0.53 cm^3 g^{-1}, respectively (Table S2).

3.3. Fabrication of sulfur cathodes in large dimension

Large-scale sulfur cathodes with high sulfur loading are simply manufactured without the sulfur infiltration step by directly employing the PEI_KB and a polar PAA binder with sulfur (Fig. 4a). A large-scale sulfur cathode (70×6 cm^2) with a high sulfur loading of > 4.3 mg cm^{-2} is fabricated in a single step via simple slurry preparation process. Sulfur loading amount is calculated by ($W_{cathode}$ x f_S)/$A_{cathode}$. $W_{cathode}$ is the weight of cathode without the weight of Al current collector, f_S is the fraction of sulfur in cathode and $A_{cathode}$ is the area of cathode. The solid structural stability of the PEI_KB-PAA cathode could be attributed to the following interactions. First, the polar properties of both PEI_KB and PAA provide a uniform dispersion of PEI_KB particles in PAA solution, which yields good uniformity of the cathode. Second, the interaction between the amine group of PEI_KB and the carboxyl group of PAA can enhance the adhesion [39]. Third, the carboxyl group of the PAA binder can react with the hydroxyl group of native Al_2O_3
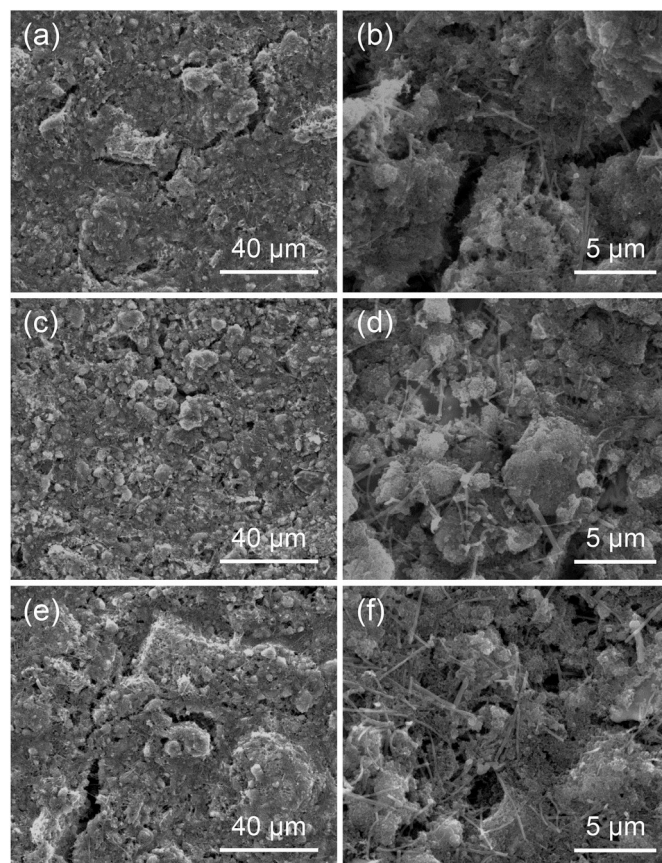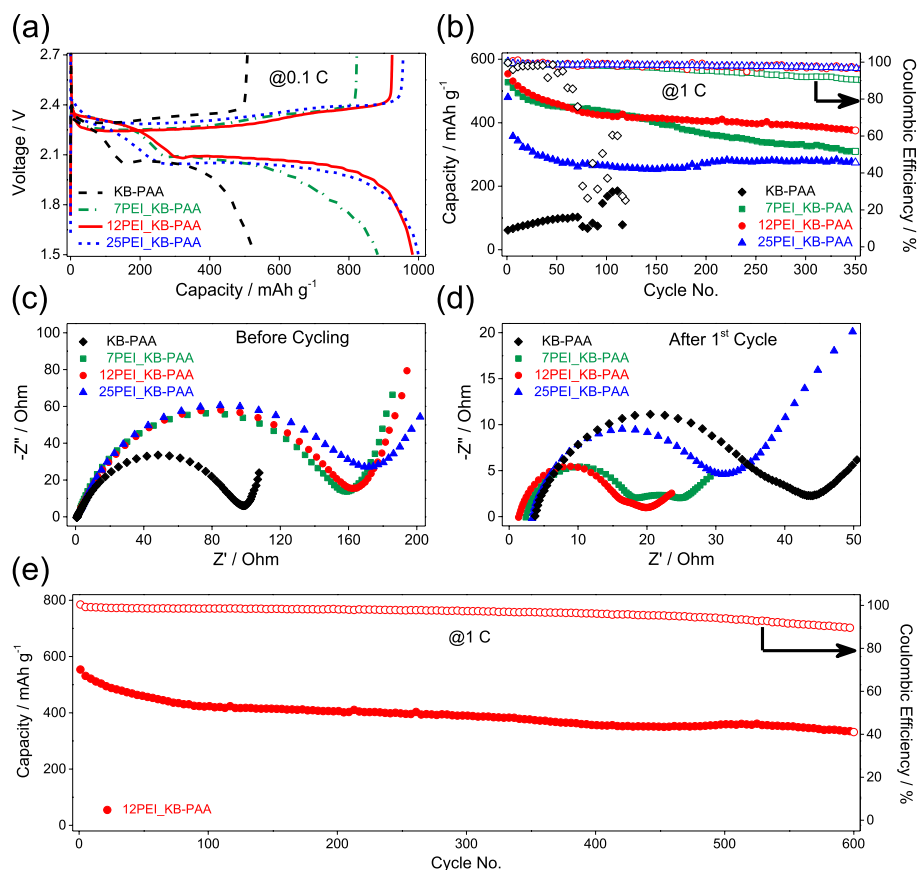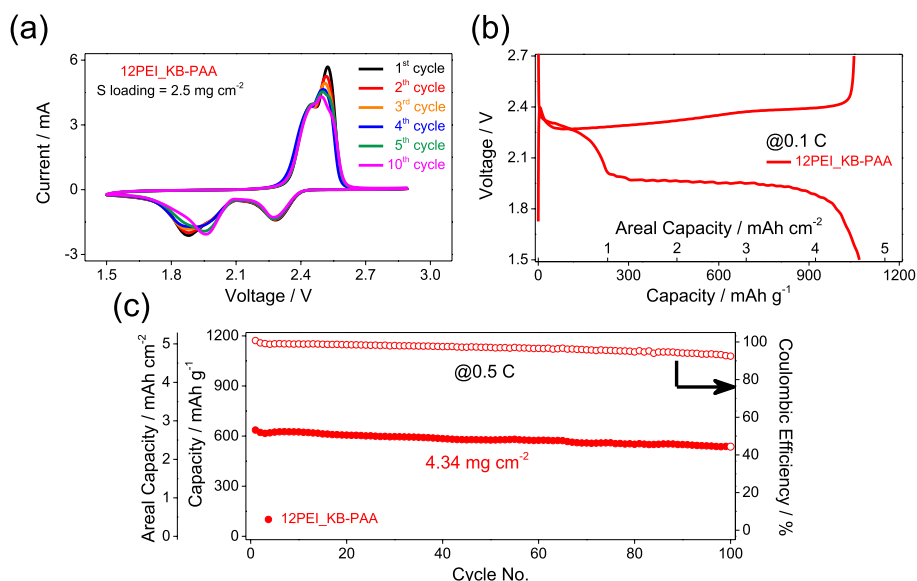

Fig. 5. Low (left column) and high (right column) magnified SEM images of (a, b) 7PEI_KB-PAA, (c, d) 12PEI_KB-PAA, and (e, f) 25PEI_KB-PAA cathodes.

layer on Al current collector via chemical bond to ensure robust contact between the cathode and current collector [40], which is similar to the interaction observed for a Si anode using PAA binder with a Cu current collector [41]. Based on these desirable features, the PEI_KB-PAA cathode demonstrates better structural stability than KB-PAA compared under same condition of sulfur loading amount (Fig. 4b and c). Moreover, the cathode with PAA binder shows better cathode structural

Fig. 6. The electrochemical properties of *x*PEI_KB-PAA (*x* = 7, 12, 25) KB-PAA (a) initial discharge-charge curves after precycling at 0.1C and (b) subsequent cycle performance at 1C. Nyquist plots of *x*PEI_KB-PAA (*x* = 7, 12, 25) and KB-PAA (c) before cycling and (d) after the 1st cycle. (e) Prolonged long-term stability of 12PEI_KB-PAA cathode at 1C. (S loading of all cathodes = 2.7 mg cm^{-2}).
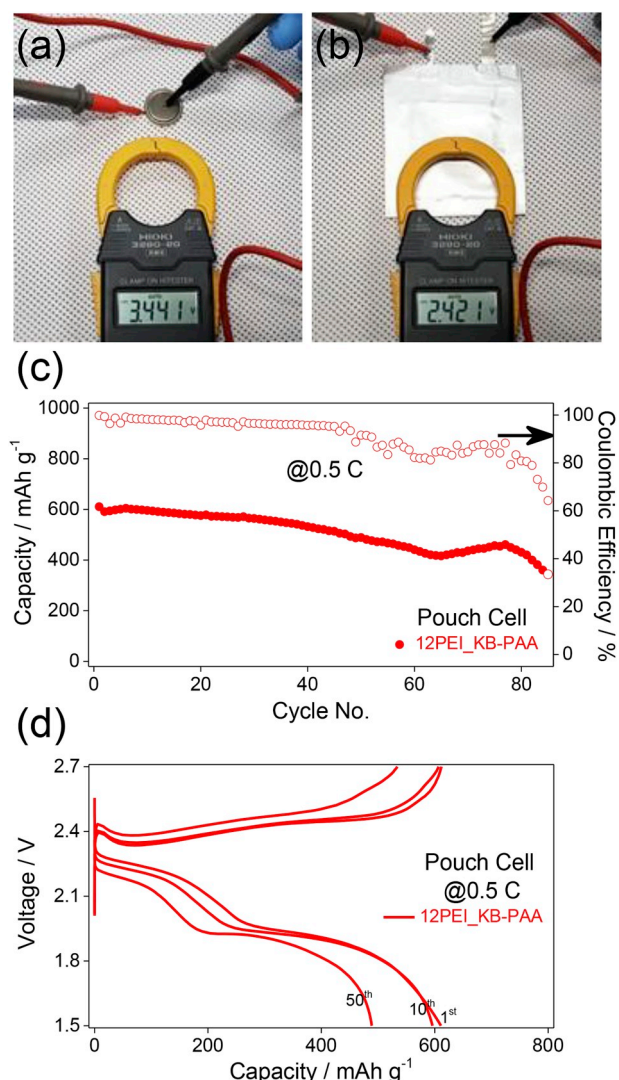

Fig. 7. (a) Cyclic voltammetry of 12PEI_KB-PAA. The electrochemical characteristics of 12PEI_KB-PAA (S loading = 4.34 mg cm^{-2}) cathode: (b) initial discharge-charge curves after precycling at 0.1C, (c) subsequent cycle performance based on both specific capacity and areal capacity at 0.5C.

quality than that obtained with PVdF binder (Fig. S4) due to its superior adhesion [41,42]. Notwithstanding the excellent properties of PAA with PEI-KB, fissuring and delamination of the cathode occur when KB is used (Fig. 4c). This fissure formation results from the aggregation of KB particles and uptake of an excessive amount of solvent, which causes inefficient binding interaction and volume shrinkage during the casting process. Accordingly, the SEM images of all *x*PEI_KB-PAA cathodes (*x* = 7, 12, and 25) show compact and stable integrity (Fig. 5).

3.4. Electrochemical measurements

The galvanostatic electrochemical cycling performance of various *x*PEI_KB-PAA cathodes (*x* = 7, 12, and 25, S loading = 2.7 mg cm^{-2}) is examined first to optimize the content ratio of PEI (Fig. 6). By introducing PEI functionalization, both discharge capacity and cycle performance are improved. The 1st discharge capacities during 0.1C precycling of the 7-, 12-, and 25PEI_KB-PAA cathodes are 882.5, 983.0, and 999.4 mAh g^{-1}, respectively, which show a tendency of increased

Fig. 8. The digital photographs measuring OCV of (a) coin cell and (b) pouch cell. The electrochemical performance of 12PEI_KB-PAA with pouch-type cell at 0.5C: (c) cycle performance and (d) discharge-charge curves during cycling.

capacity in proportion to an increased PEI amount (Fig. 6a). 25PEI_KB-PAA cathode demonstrates a larger polarization than that of other cathodes; the increase in polarization is achieved by increased internal resistance, which is attributed to an increment of insulating PEI in PEI_KB [8]. Whereas 12PEI_KB-PAA cathode presents the smallest polarization, which confirms the optimized PEI composition. After 350 cycles at 1C, the 12PEI_KB-PAA cathode presents the best electrochemical cycling performance compared with that of the other cathodes (Fig. 6b). The 25PEI_KB-PAA cathode exhibits the lowest discharge capacity; this is caused by the insulating properties of the excess PEI [43]. Although the 7PEI_KB-PAA cathode has a discharge capacity similar to that of 12PEI_KB-PAA during the initial 150 cycles, its capacity retention and Coulombic efficiency subsequently deteriorate compared with that of 12PEI_KB-PAA. This difference in capacity and Coulombic efficiency might result from the insufficiency of amine functional groups, which play an essential role in capturing the LiPSs species during long-term cycling. Further EIS analysis is performed to corroborate the optimum ratio of PEI (Fig. 6c and d). Nyquist plots consist of an intercept in the high-frequency region on the real Z axis, a depressed semicircle in the high-frequency region, and an inclined line in the low-frequency region; these components correspond to the electrolyte resistance (R_e), the charge transfer resistance (R_{ct}), and the Li$^+$ ion

diffusion process, respectively. The fitting results are listed in Table S3, corresponding with the cycle performance at 1C. After the 1st discharge-charge cycle, the R_{ct} value of KB-PAA becomes the largest and it might be induced by the presence considerable amount of elemental sulfur in cathode, which is unincorporated the reaction. Meanwhile, the R_{ct} value of 12PEI_KB-PAA is smaller than that of the other cathodes after the 1st discharge-charge cycle, even though the R_{ct} of 12PEI_KB-PAA before cycling is considerably larger than that of KB-PAA, which arises from the greater insulation provided by the increased amount of PEI coating material. Additional semicircle in the middle-frequency region of 7PEI_KB-PAA is found after the 1st cycle as a result of the remaining Li$_2$S passivation layer in cathode [43,44]. Whereas the semicircle in the middle-frequency region is not found in 25PEI_KB-PAA due to the uniform Li$_2$S distribution and following transformation to sulfur enabled by enough PEI during the 1st cycle. The optimum 12PEI_KB-PAA cathode with the smallest R_{ct} and imperceptible semicircle in the middle-frequency region presents prolonged cycling stability over 600 cycles under a 1C discharge-charge rate (Fig. 6e). Generation of surface passivation layer and corrosion on Li metal anode surface from shuttle reaction as cycles progress results in gradual decreasing of the Coulombic efficiency after 500 cycles.

We investigate further electrochemical properties of the optimal 12PEI_KB-PAA cathode at higher areal sulfur loading of 4.34 mg cm^{-2} (Fig. 7). The CV results of the 12PEI_KB-PAA cathode present the typical two reduction peaks and one oxidation peak of Li−S cells (Fig. 7a). The CV measurements indicate good reversibility of this cathode during 10 cycles, despite a slight decrease in the anodic current value as the cycle progresses. The galvanostatic voltage profile of the 12PEI_KB-PAA cathode after precycling at 0.1C displays two discharge plateaus and one charge plateau, which are identical to the CV results (Fig. 7b). The initial areal discharge capacity at 0.1C precycling of 12PEI_KB-PAA is 4.63 mAh cm^{-2}, which is much higher than the capacity of 1.11 mAh cm^{-2} and 0.97 mAh cm^{-2} observed for KB-PAA (S loading = 2.38 mg cm^{-2}) and KB-PVdF (S loading = 0.74 mg cm^{-2}), respectively (Fig. S5). Additionally, 12PEI_KB-PAA displays improved cycle performance at 0.5C (Figs. 7c and S6a) with a retention ratio of 85% for over 100 cycles. The enhanced electrochemical performance of 12PEI_KB-PAA compared with those of KB-PAA result from the aforementioned improved structural stability of the cathode. Uniformly distributed PEI_KB particles can prevent the aggregation of cathode materials and provide stable electrical pathways. Even though the polarization in voltage profiles of 12PEI_KB-PAA during cycling at 0.5C increases due to the high sulfur loading, the well-developed two discharge plateaus remains stable more than 100 cycles (Fig. S7). Above all, from the areal capacity point of view, the 12PEI_KB-PAA cathode demonstrates a significantly enhanced areal capacity, approximately four times larger than that of KB-PAA and five times larger than that of KB-PVdF, during cycling at 0.5C (Fig. 7c and S6). Pouch-type cell with single layer of cathode and anode is fabricated with a size of 3 × 4 cm^2 to verify the benefited scalability of PEI_KB-PAA cathode (Fig. 8). After 12 h rest time of the pouch cell, open circuit voltage (OCV) of the pouch cell is lower than that of the coin cell (Fig. 8a and b) by the self-discharge of the pouch cell that promoted from the expanded cathode area [45]. The pouch cell exhibits an initial specific discharge capacity of 610.8 mAh g^{-1} at 0.5C and lasts a cycle life over 80 cycles (Fig. 8c). The pouch cell has well-retained discharge capacity and presents a reliable voltage profiles until 50 cycles (Fig. 8d). However, the Coulombic efficiency is deteriorated over 50 cycle and the discharge capacity is rapidly decreased over 80 cycles. The curtailed cycle life compared to the coin cell is resulted from not only irreversible LiPSs dissolution but also the disparity in pouch cell and coin cell from exacerbated Li metal anode [46].

4. Conclusions

Commercial KB has a very high SSA and can be used for a variety of

energy storage systems, including Li−S batteries. However, KB was not suitable for sulfur host materials because of unstable cathode formation with fissures and delamination caused by aggregation and volume shrinkage after cathode drying. In addition, high SSA of KB is generally advantageous for accomplishing high discharge capacity but is undesirable in terms of capacity maintenance. However, the surface functionalization of KB with PEI and utilization of a PAA binder rendered the pragmatic and productive manufacturing of the high energy sulfur cathode with a large scale and the improved capacity retention. On the basis of the robust interaction between PEI_KB and the polar PAA binder, it became possible to fabricate a high-sulfur-loading cathode with a loading of $> 4.3\,\mathrm{mg\,cm^{-2}}$ and a large scale of $70 \times 6\,\mathrm{cm^2}$ in a single step. Furthermore, this practicably manufactured high-energy-density cathode exhibited a discharge capacity of 1,067.6 mAh g^{-1} (equivalent to an areal capacity of 4.63 mAh cm^{-2}) at 0.1C during initial precycling and excellent cycling stability over 100 cycles at 0.5C (capacity retention of 85% and average Coulombic efficiency of 96.8%). We believed that facile cathode fabrication methods developed here supported by the simple and scalable synthesis of PEI_KB sulfur host and with polar PAA binder pave the way of constructing pragmatic Li−S batteries.

Acknowledgments

Appendix A. Supplementary data

Supplementary data to this article can be found online at https://doi.org/10.1016/j.jpowsour.2019.02.093.

References

[1] X. Ji, K.T. Lee, L.F. Nazar, A highly ordered nanostructured carbon-sulphur cathode for lithium-sulphur batteries, Nat. Mater. 8 (2009) 500–506, https://doi.org/10.1038/nmat2460.

[2] P.G. Bruce, S.A. Freunberger, L.J. Hardwick, J.-M. Tarascon, Li–O2 and Li–S batteries with high energy storage, Nat. Mater. 11 (2012) 19–29, https://doi.org/10.1038/nmat3237.

[3] Z.W. Seh, W. Li, J.J. Cha, G. Zheng, Y. Yang, M.T. McDowell, P.C. Hsu, Y. Cui, Sulphur-TiO 2 yolk-shell nanoarchitecture with internal void space for long-cycle lithium-sulphur batteries, Nat. Commun. 4 (2013) 1331, https://doi.org/10.1038/ncomms2327.

[4] L. Sun, M. Li, Y. Jiang, W. Kong, K. Jiang, J. Wang, S. Fan, Sulfur nanocrystals confined in carbon nanotube network as a binder-free electrode for high performance lithium sulfur batteries, Nano Lett. 14 (2014) 4044–4049, https://doi.org/10.1021/nl501486n.

[5] M.-K. Song, Y. Zhang, E.J. Cairns, A long-life, high-rate lithium/sulfur cell: a multifaceted approach to enhancing cell performance, Nano Lett. 13 (2013) 5891–5899, https://doi.org/10.1021/nl402793z.

[6] K. Park, J.H. Cho, J.-H. Jang, B.-C. Yu, A.T. De La Hoz, K.M. Miller, C.J. Ellison, J.B. Goodenough, Trapping lithium polysulfides of a Li–S battery by forming lithium bonds in a polymer matrix, Energy Environ. Sci. 8 (2015) 2389–2395, https://doi.org/10.1039/C5EE01809A.

[7] S. Xin, L. Gu, N.-H. Zhao, Y.-X. Yin, L.-J. Zhou, Y.-G. Guo, L.-J. Wan, Smaller sulfur molecules promise better lithium-sulfur batteries, J. Am. Chem. Soc. 134 (2012) 18510–18513, https://doi.org/10.1021/ja308170k.

[8] M.-S. Kim, J. Jeong, W. Il Cho, W. Kim, Synthesis of graphitic ordered mesoporous carbon with cubic symmetry and its application in lithium-sulfur batteries, Nanotechnology 27 (2016) 125401, https://doi.org/10.1088/0957-4484/27/12/125401.

[9] L. Ma, H.L. Zhuang, S. Wei, K.E. Hendrickson, M.S. Kim, G. Cohn, R.G. Hennig, L.A. Archer, Enhanced Li-S batteries using amine-functionalized carbon nanotubes in the cathode, ACS Nano 10 (2016) 1050–1059, https://doi.org/10.1021/acsnano.5b06373.

[10] E.S. Shin, M.-S. Kim, W. Il Cho, S.H. Oh, Sulfur/graphitic hollow carbon sphere nano-composite as a cathode material for high-power lithium-sulfur battery, Nanoscale Res. Lett. 8 (2013) 343, https://doi.org/10.1186/1556-276X-8-343.

[11] N. Jayaprakash, J. Shen, S.S. Moganty, A. Corona, L.A. Archer, Porous hollow carbon@sulfur composites for high-power lithium-sulfur batteries, Angew. Chem. Int. Ed. 50 (2011) 5904–5908, https://doi.org/10.1002/anie.201100637.

[12] B. Liu, Y. Jia, J. Li, S. Yin, C. Yuan, Z. Hu, L. Wang, Y. Li, J. Xu, Safety issues caused

[13] by internal short circuits in lithium-ion batteries, J. Mater. Chem. A. 6 (2018) 21475–21484, https://doi.org/10.1039/C8TA08997C.

[13] Y. Jia, S. Yin, B. Liu, H. Zhao, H. Yu, J. Li, J. Xu, Unlocking the coupling mechanical-electrochemical behavior of lithium-ion battery upon dynamic mechanical loading, Energy 166 (2019) 951–960, https://doi.org/10.1016/j.energy.2018.10.142.

[14] R. Fang, S. Zhao, Z. Sun, D.W. Wang, H.M. Cheng, F. Li, More reliable lithium-sulfur batteries: status, solutions and prospects, Adv. Mater. 29 (2017) 1606823, https://doi.org/10.1002/adma.201606823.

[15] D. Lv, J. Zheng, Q. Li, X. Xie, S. Ferrara, Z. Nie, L.B. Mehdi, N.D. Browning, J.G. Zhang, G.L. Graff, J. Liu, J. Xiao, High energy density lithium-sulfur batteries: challenges of thick sulfur cathodes, Adv. Energy Mater. 5 (2015) 1402290, https://doi.org/10.1002/aenm.201402290.

[16] X. Yang, X. Li, K. Adair, H. Zhang, X. Sun, Structural design of lithium–sulfur batteries: from fundamental Research to practical application, Electrochem. Energy Rev. 1 (2018) 239–293, https://doi.org/10.1007/s41918-018-0010-3.

[17] L. Miao, W. Wang, K. Yuan, Y. Yang, A. Wang, A lithium-sulfur cathode with high sulfur loading and high capacity per area: a binder-free carbon fiber cloth-sulfur material, Chem. Commun. 50 (2014) 13231–13234, https://doi.org/10.1039/c4cc03410d.

[18] Z. Yuan, H.-J. Peng, J.-Q. Huang, X.-Y. Liu, D.-W. Wang, X.-B. Cheng, Q. Zhang, Hierarchical free-standing carbon-nanotube paper electrodes with ultrahigh sulfur-loading for lithium-sulfur batteries, Adv. Funct. Mater. 24 (2014) 6105–6112, https://doi.org/10.1002/adfm.201401501.

[19] L. Qie, A. Manthiram, A facile layer-by-layer approach for high-areal-capacity sulfur cathodes, Adv. Mater. 27 (2015) 1694–1700, https://doi.org/10.1002/adma.201405689.

[20] Z. Li, J.T. Zhang, Y.M. Chen, J. Li, X.W. Lou, Pie-like electrode design for high-energy density lithium-sulfur batteries, Nat. Commun. 6 (2015) 8850, https://doi.org/10.1038/ncomms9850.

[21] G. Zhou, L. Li, C. Ma, S. Wang, Y. Shi, N. Koratkar, W. Ren, F. Li, H.-M. Cheng, A graphene foam electrode with high sulfur loading for flexible and high energy Li-S batteries, Nanomater. Energy 11 (2015) 356–365, https://doi.org/10.1016/j.nanoen.2014.11.025.

[22] X. Hong, J. Jin, T. Wu, Y. Lu, S. Zhang, C. Chen, Z. Wen, A rGO-CNT aerogel covalently bonded with a nitrogen-rich polymer as a polysulfide adsorptive cathode for high sulfur loading lithium sulfur batteries, J. Mater. Chem. A. 5 (2017) 14775–14782, https://doi.org/10.1039/c7ta03552g.

[23] J. Song, M.L. Gordin, T. Xu, S. Chen, Z. Yu, H. Sohn, J. Lu, Y. Ren, Y. Duan, D. Wang, Strong lithium polysulfide chemisorption on electroactive sites of nitrogen-doped carbon composites for high-performance lithium-sulfur battery cathodes, Angew. Chem. Int. Ed. 54 (2015) 4325–4329, https://doi.org/10.1002/anie.201411109.

[24] H.J. Peng, J.Q. Huang, X.B. Cheng, Q. Zhang, Review on high-loading and high-energy lithium–sulfur batteries, Adv. Energy Mater. 7 (2017) 1700260, https://doi.org/10.1002/aenm.201700260.

[25] Y. Yoo, J. Park, M.S. Kim, W. Kim, Development of 2.8 V Ketjen black supercapacitors with high rate capabilities for AC line filtering, J. Power Sources 360 (2017) 383–390, https://doi.org/10.1016/j.jpowsour.2017.06.032.

[26] D. Wang, D. Wang, W. Xu, D. Wang, R.E. Williford, J. Liu, J.-G. Zhang, Optimization of air electrode for Li/air batteries, J. Electrochem. Soc. 157 (2010) A487–A492, https://doi.org/10.1149/1.3314375.

[27] Y. Ma, H. Zhang, B. Wu, M. Wang, X. Li, H. Zhang, Lithium sulfur primary battery with super high energy density: based on the cauliflower-like structured C/S cathode, Sci. Rep. 5 (2015) 14949, https://doi.org/10.1038/srep14949.

[28] T. Yim, S.H. Han, N.H. Park, M.S. Park, J.H. Lee, J. Shin, J.W. Choi, Y. Jung, Y.N. Jo, J.S. Yu, K.J. Kim, Effective polysulfide rejection by dipole-aligned BaTiO3 coated separator in lithium–sulfur batteries, Adv. Funct. Mater. 26 (2016) 7817–7823, https://doi.org/10.1002/adfm.201602498.

[29] S. Zhang, P. Kang, S. Ubnoske, M.K. Brennaman, N. Song, R.L. House, J.T. Glass, T.J. Meyer, Polyethylenimine-enhanced electrocatalytic reduction of CO2 to formate at nitrogen-doped carbon nanomaterials, J. Am. Chem. Soc. 136 (2014) 7845–7848, https://doi.org/10.1021/ja5031529.

[30] S. Foillard, G. Zuber, E. Doris, Polyethylenimine–carbon nanotube nanohybrids for siRNA-mediated gene silencing at cellular level, Nanoscale 3 (2011) 1461–1464, https://doi.org/10.1039/c0nr01005g.

[31] Y.-E. Yoo, J. Park, W. Kim, Understanding and controlling the rest potential of carbon nanotube-based supercapacitors for energy density enhancement, Appl. Surf. Sci. 433 (2018) 765–771, https://doi.org/10.1016/j.apsusc.2017.10.044.

[32] M.S. Kim, M.-S. Kim, V. Do, Y.R. Lim, I.W. Nah, L.A. Archer, W. Il Cho, Designing solid-electrolyte interphases for lithium sulfur electrodes using ionic shields, Nanomater. Energy 41 (2017) 573–582, https://doi.org/10.1016/j.nanoen.2017.10.018.

[33] A.C. Ferrari, Raman spectroscopy of graphene and graphite: disorder, electron-phonon coupling, doping and nonadiabatic effects, Solid State Commun. 143 (2007) 47–57, https://doi.org/10.1016/j.ssc.2007.03.052.

[34] A.C. Ferrari, D.M. Basko, Raman spectroscopy as a versatile tool for studying the properties of graphene, Nat. Nanotechnol. 8 (2013) 235–246, https://doi.org/10.1038/nnano.2013.46.

[35] R. Bajpai, S. Roy, N. Kulshrestha, J. Rafiee, N. Koratkar, D.S. Misra, Graphene supported nickel nanoparticle as a viable replacement for platinum in dye sensitized solar cells, Nanoscale 4 (2012) 926–930, https://doi.org/10.1039/C2NR11127F.

[36] K.S.W. Sing, Reporting physisorption data for gas/solid systems with special reference to the determination of surface area and porosity, Pure Appl. Chem. 57 (1985) 603–619, https://doi.org/10.1351/pac198557040603.

[37] T. Soboleva, X. Zhao, K. Malek, Z. Xie, T. Navessin, S. Holdcroft, On the micro-,

meso-, and macroporous structures of polymer electrolyte membrane fuel cell catalyst layers, ACS Appl. Mater. Interfac. 2 (2010) 375–384, https://doi.org/10.1021/am900600y.

[38] S. Lowell, J.E. Shields, M.A. Thomas, M. Thommes, Characterization of Porous Solids and Powders: Surface Area, Pore Size and Density, Springer, Netherlands, 2004, https://doi.org/10.1007/978-1-4020-2303-3.

[39] L. Wang, Z. Dong, D. Wang, F. Zhang, J. Jin, Covalent bond glued sulfur nanosheet-based cathode integration for long-cycle-life Li-S batteries, Nano Lett. 13 (2013) 6244–6250, https://doi.org/10.1021/nl403715h.

[40] S. Pletincx, L. Trotochaud, L. Fockaert, J.M.C. Mol, A.R. Head, O. Karslıoğlu, H. Bluhm, H. Terryn, T. Hauffman, In situ characterization of the initial effect of water on molecular interactions at the interface of organic/inorganic hybrid systems, Sci. Rep. 7 (2017) 45123, https://doi.org/10.1038/srep45123.

[41] A. Magasinski, B. Zdyrko, I. Kovalenko, B. Hertzberg, R. Burtovyy, C.F. Huebner, T.F. Fuller, I. Luzinov, G. Yushin, Toward efficient binders for Li-ion battery Si-based anodes: polyacrylic acid, ACS Appl. Mater. Interfac. 2 (2010) 3004–3010, https://doi.org/10.1021/am100871y.

[42] Z. Zhang, T. Zeng, Y. Lai, M. Jia, J. Li, A comparative study of different binders and

their effects on electrochemical properties of LiMn2O4 cathode in lithium ion batteries, J. Power Sources 247 (2014) 1–8, https://doi.org/10.1016/j.jpowsour.2013.08.051.

[43] W. Li, Q. Zhang, G. Zheng, Z.W. Seh, H. Yao, Y. Cui, Understanding the role of different conductive polymers in improving the nanostructured sulfur cathode performance, Nano Lett. 13 (2013) 5534–5540, https://doi.org/10.1021/nl403130h.

[44] L. Yuan, X. Qiu, L. Chen, W. Zhu, New insight into the discharge process of sulfur cathode by electrochemical impedance spectroscopy, J. Power Sources 189 (2009) 127–132, https://doi.org/10.1016/j.jpowsour.2008.10.033.

[45] S.M. Al-Mahmoud, J.W. Dibden, J.R. Owen, G. Denuault, N. Garcia-Araez, A simple, experiment-based model of the initial self-discharge of lithium-sulphur batteries, J. Power Sources 306 (2016) 323–328, https://doi.org/10.1016/j.jpowsour.2015.12.031.

[46] X.B. Cheng, C. Yan, J.Q. Huang, P. Li, L. Zhu, L. Zhao, Y. Zhang, W. Zhu, S.T. Yang, Q. Zhang, The gap between long lifespan Li-S coin and pouch cells: the importance of lithium metal anode protection, Energy Storage Mater. 6 (2017) 18–25, https://doi.org/10.1016/j.ensm.2016.09.003.